European Journal of Medicinal Chemistry 44 (2009) 2822–2827

Contents lists available at ScienceDirect

European Journal of Medicinal Chemistry

journal homepage: http://www.elsevier.com/locate/ejmech

Original article

CoMFA and docking studies of 2-phenylindole derivatives with anticancer activity

Si Yan Liao, Li Qian, Ti Fang Miao, Hai Liang Lu, Kang Cheng Zheng*

School of Chemistry and Chemical Engineering, Zhongshan (Sun Yat-Sen) University, Guangzhou 510275, China

ARTICLE INFO

Article history:
Received 11 July 2008
Received in revised form
16 November 2008
Accepted 15 December 2008
Available online 25 December 2008

Keywords:
2-Phenylindole derivative
Anticancer activity
QSAR
CoMFA
Docking study

ABSTRACT

Three-dimensional (3D) quantitative structure–activity relationship (QSAR) and docking studies of 43 tubulin inhibitors, 2-phenylindole derivatives with anticancer activity against human breast cancer cell line MDA-MB 231, have been carried out. The established 3D-QSAR model from the comparative molecular field analysis (CoMFA) in training set shows not only significant statistical quality, but also satisfying predictive ability, with high correlation coefficient value ($R^2 = 0.910$) and cross-validation coefficient value ($q^2 = 0.705$). Moreover, the predictive ability of the CoMFA model was further confirmed by a test set, giving the predictive correlation coefficient (R^2_{pred}) of 0.688. Based on the CoMFA contour maps and docking analyses, some key structural factors responsible for anticancer activity of this series of compounds were revealed as follows: the substituent R_1 should have higher electronegativity; the substituent R_2 should be linear alkyl with four or five carbon atoms in length; and the substituent R_3 should be selected to OCH_3-kind group whereas should not be selected to CF_3-kind group. Meanwhile, the interaction information between target and ligand was presented in detail. Such results can offer some useful theoretical references for understanding the action mechanism, designing more potent inhibitors and predicting their activities prior to synthesis.

1. Introduction

Microtubules, cylindrical protein polymers composed of α- and β-tubulin heterodimers, are essential for many cellular functions, such as maintenance of cellular shape, intracellular transport and separation of chromosomes during mitosis [1,2]. Inhibition of microtubule formation leads to mitotic arrest and promotes vascular disruption, eventually leading to cell death by apoptosis [3,4]. Hence, tubulin is one of the most common and strategic targets for development of new anticancer drugs [5].

Paclitaxel, a microtubule-stabilizing agent binding to the fully formed microtubules and preventing depolymerization of the tubulin subunits, and Vinblastine binding to the tubulin monomers and inhibiting their polymerization into microtubules, are proapoptotic chemotherapeutic agents and successfully prescribed in anticancer therapies [6]. However, these drugs exhibit drug resistance and dose-limiting neurologic and bone marrow toxicity [7,8]. The colchicine-binding site located on the monomeric unpolymerized α/β-tubulin represents another potential tubulin target for the development of apoptosis inducing chemotherapeutic agents [9]. Combretastatin A-4 phosphate (CA-4P) [10], water-soluble prodrug of combretastatin A-4 (CA-4), inhibits tubulin polymerization by binding at the colchicine site and is currently used in clinical trials. In addition to its potent cytotoxicity, CA-4 is one of the few tubulin targeting agents reported to have selective vascular-disrupting activity [11,12]. Recently, von Angerer and coworkers have synthesized a series of 2-phenylindole derivatives and assessed their anticancer activities in human breast cancer cell lines [13–15]. They found that these compounds prevent the polymerization of the α/β-tubulin dimers to functional microtubules by binding to the colchicine-binding site and all have pronounced cytotoxicity, demonstrating the great potential of developing 2-phenylindole derivatives as a new class of anticancer drug. However, a more detailed investigation about how the structural features of these compounds influence their anticancer activities and the inhibition mechanisms of these compounds remains largely unknown. So it is very significant work to investigate the quantitative structure–activity relationship (QSAR) and inhibition mechanism of this kind of compound.

QSAR, which quantitatively correlates the variations in biological activity with the properties or molecular structures, is one of the most effective approaches for understanding action mechanisms

* Corresponding author. Tel.: +86 20 84110696; fax: +86 20 84112245.
E-mail address: ceszkc@mail.sysu.edu.cn (K.C. Zheng).

0223-5234/$ – see front matter © 2008 Elsevier Masson SAS. All rights reserved.
doi:10.1016/j.ejmech.2008.12.020

drugs and designing new drugs [16,17]. Nowadays, comparative molecular field analysis (CoMFA) has been successfully used in modern drug design. It is a useful technique in understanding the pharmacological properties of studied compounds, because not only CoMFA model is visualized, but also the obtained steric and electrostatic maps can help to understanding the detail of interaction between the ligand and the active site of receptor [18,19]. Docking analysis is also a useful methodology to further study the interaction mechanism, since it can offer vivid interaction picture between a ligand and an acceptor [20,21]. Therefore, a combined 3D-QSAR and docking study could offer more insight into understanding the QSAR, the structural features of active site of protein and the detail of protein–inhibitor interactions, and thus could more effectively direct the design of new potential inhibitors.

In this work, CoMFA and docking studies of 43 tubulin inhibitors, 2-phenylindole derivatives with anticancer activity against human breast cancer cell line MDA-MB 231 [13–15], were carried out. The purpose of this article focuses to establish an optimal 3D-QSAR model for these compounds by using the CoMFA method and explore the inhibition mechanism via docking analysis combined with 3D-QSAR. We expect that the theoretical results can offer some useful references for the experimenters in the design of new anticancer drugs and the action mechanism analysis.

2. Computational methods

2.1. The studied compounds and their biological activity data

A series of 2-phenylindole derivatives with well-expressed cytotoxicity against human breast cancer cell line MDA-MB 231 [13–15], were selected to perform the present study. The structural formula of the studied compounds is shown in Fig. 1. The total set of these inhibitors was divided into a training set composed of 35 compounds and a test set composed of 8 compounds. The test compounds were selected manually so that the structural diversity and wide range of activities in the data set were considered. We used the literature data for IC_{50} which is defined as the value of the necessary molar concentration of compound to cause 50% growth inhibition against the human MDA-MB 231 breast cancer cell line. The corresponding values are listed in Table 1. All original IC_{50} values were converted to negative logarithm of IC_{50} (pIC_{50}) used as dependent variable in the CoMFA study.

2.2. Molecular modeling

CoMFA study was performed using SYBYL 6.9 molecular modeling software [22] running on an SGI R2400 workstation. All parameters used in CoMFA were default except for explained.

Active conformation selection is a key step for CoMFA analysis. Since the crystal structure of complex of tubulin with one of these compounds is not available, conformation search was performed in Chem3D software to discover the global energy-minimum conformation for the most active compound **31** by rotating rotatable bonds. Then the conformation with minimum energy was further optimized by the Gaussian 03 program package [23] using semi-empirical quantum-chemical PM3 calculation. The rest of the molecules were built by changing the substitutions of compound **31** and were minimized with the same way. Finally, Gasteiger–Hückel charges were assigned to all the molecules.

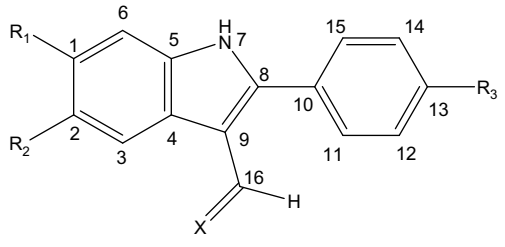

Fig. 1. Molecular structure and numbering of studied 2-phenylindole derivatives.

Table 1
Structures and experimental anticancer activities (against human breast cancer cell line MDA-MB 231) of the 2-phenylindole derivatives.

No.	R_1	R_2	R_3	X	IC_{50} (nM)	pIC_{50}
1	H	H	H	$C(CN)_2$	430	6.367
2	H	H	OMe	$C(CN)_2$	720	6.143
3[a]	H	OMe	OMe	$C(CN)_2$	590	6.229
4	OMe	H	OMe	$C(CN)_2$	260	6.585
5	H	F	OMe	$C(CN)_2$	400	6.398
6	F	H	OMe	$C(CN)_2$	280	6.553
7	OMe	H	Me	$C(CN)_2$	180	6.745
8[a]	H	Me	OMe	$C(CN)_2$	280	6.553
9	Cl	Me	OMe	$C(CN)_2$	75	7.125
10	H	*n*-Pr	OMe	$C(CN)_2$	83	7.081
11	H	*i*-Pr	OMe	$C(CN)_2$	210	6.678
12	H	*n*-Bu	OMe	$C(CN)_2$	26	7.585
13	H	*n*-Pentyl	OMe	$C(CN)_2$	42	7.377
14	H	*n*-Hexyl	OMe	$C(CN)_2$	46	7.337
15	H	*n*-Bu	Me	$C(CN)_2$	65	7.187
16	H	*n*-Bu	Et	$C(CN)_2$	76	7.119
17	H	*n*-Bu	CF_3	$C(CN)_2$	56	7.252
18	H	*n*-Pentyl	CF_3	$C(CN)_2$	78	7.108
19	H	*n*-Hexyl	CF_3	$C(CN)_2$	150	6.824
20	H	OMe	OMe	O	260	6.585
21	OMe	H	OMe	O	35	7.456
22	F	H	OMe	O	59	7.229
23	H	F	OMe	O	540	6.268
24	Cl	H	OMe	O	27	7.569
25	Cl	Me	OMe	O	26	7.585
26[a]	H	Me	OMe	O	86	7.066
27	H	Pr	OMe	O	20	7.699
28	H	*n*-Bu	OMe	O	6.7	8.174
29	H	*sec*-Bu	OMe	O	72	7.143
30	H	*t*-Bu	OMe	O	280	6.553
31	H	*n*-Pentyl	OMe	O	5.5	8.260
32[a]	H	*n*-Hexyl	OMe	O	7.4	8.131
33	OMe	OMe	OMe	O	220	6.658
34[a]	OMe	H	Me	O	31	7.509
35	H	Me	Me	O	48	7.319
36[a]	H	*n*-Bu	Me	O	34	7.469
37	H	*n*-Bu	Et	O	27	7.569
38[a]	H	Et	*n*-Bu	O	300	6.523
39	H	*n*-Bu	CF_3	O	33	7.481
40	H	*n*-Pentyl	CF_3	O	42	7.377
41	H	*n*-Hexyl	CF_3	O	43	7.367
42	OMe	H	H	O	240	6.620
43[a]	H	H	H	O	420	6.377

[a] Compounds in the test set.

2.3. Alignment

Structural alignment is considered as one of the most sensitive parameters in CoMFA analysis. The accuracy of the prediction of CoMFA model and reliability of the contour maps are directly dependent on the structural alignment rule [24]. The most active compound **31** was used as a template for superimposition, and the common fragment (the atoms numbered from 1 to 16) shown in Fig. 1 was selected for alignment and all the molecules were aligned on it. The aligned compounds are shown in Fig. 2.

2.4. Generation of CoMFA field

Models of steric and electrostatic fields for CoMFA were based on both Lennard–Jones and Coulombic potentials [25]. Steric and electrostatic energies were calculated using a sp^3 carbon atom with

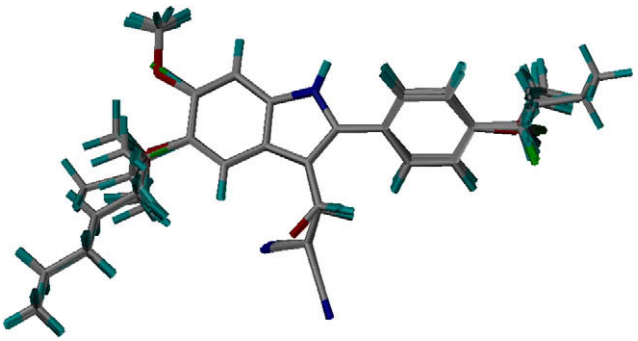

Fig. 2. Alignment of the 43 studied molecules.

van der Waals radius of 1.52 Å, charge of +1.0, and grid spacing of 2.0 Å. The CoMFA cutoff values were set to 30 kcal/mol for both steric and electrostatic fields.

2.5. Partial least squares (PLS) analysis and validation of 3D-QSAR model

Partial least squares (PLS) analysis was used to construct a linear correlation between the 3D-fields (independent variables) and the anticancer activity values (dependent variables). To select the best model, the cross-validation analysis was performed using the leave-one-out (LOO) method in which one compound was removed from the data set and its activity was predicted using the model built from rest of the data set [26]. It results in the cross-validation correlation coefficient (q^2) and the optimum number of components *N*. The non-cross-validation was performed with a column filter value of 2.0 to speed up the analysis and reduce the noise. To further assess the robustness and the statistical validity of the obtained models, bootstrapping analysis for 100 runs was performed.

To assess the predictive abilities of the CoMFA model derived by the training set, biological activities of an external test set composed of eight compounds were predicted. The predictive ability of the model is expressed by the predictive correlation coefficient R^2_{pred}, calculated by the formula: $R^2_{\text{pred}} = (\text{SD-PRESS})/\text{SD}$, where SD is the sum of the squared deviations between the biological activities of the test set compounds and mean activity of the training set compounds, and PRESS is the sum of squared deviations between experimental and predicted activities of the test set compounds.

2.6. Molecular docking

To locate the appropriate binding orientations and conformations of these 2-phenylindole derivatives interacting with tubulin, docking study for all studied compounds was performed with the DOCK 6.0 program. All parameters used in docking were default except for explained.

The X-ray crystal structure of tubulin taken from the Protein Data Bank (pdb Id: 1SA0) was used to dock. Beginning of docking, all the water molecules and subunits were removed, and add hydrogen atoms and AMBER7FF99 charges to the protein. Next, only hydrogen positions were minimized in 10,000 cycles with Powell method in SYBYL 6.9 [22]. Then the surface of protein was calculated with the Dms program. To obtain binding sites, some spheres were generated and selected by Sphgen module. At last, all 2-phenylindole derivatives were flexibly docked into the binding sites. The box size, the grid space, energy cutoff distance, and max orientation were set as 8 Å, 0.3 Å, 9999 Å and 1000 Å, respectively.

3. Results and discussion

3.1. 3D-QSAR model

The 3D-QSAR model was established from CoMFA analysis and its statistical parameters are listed in Table 2. For a reliable predictive model, the cross-validation coefficient q^2 should be greater than 0.5.

This CoMFA model has high R^2 (0.910), F (58.6) and q^2 (0.705), as well as small SEE (0.167), suggesting that established CoMFA model is reliable and predictive. Moreover, the R^2_{pred} value (0.688) represents that the predictive ability of the CoMFA model is good. The R^2_{bs} of 0.938 and SD_{bs} of 0.134 obtained from bootstrapping analysis (100 runs) further confirm the statistical validity and robustness of the established CoMFA model. The steric and electrostatic contributions were found to be 62.3% and 37.7%, respectively. Therefore, the steric field has a greater influence than the electrostatic field, indicating that the steric interaction of the ligand with the receptor may be a more important factor for the anticancer activity.

The calculated (in training set) and predicted (in test set) activity values and the residual values of compounds for the CoMFA model are also listed in Table 3. The plot of the calculated (predicted) pIC_{50} values versus experimental ones for the CoMFA analysis is shown in Fig. 3, in which most points are evenly distributed along the line $Y = X$, suggesting that the CoMFA model has good quality.

3.2. The validation of docking reliability

As above-mentioned, it is well-reported that the anticancer mechanism of this kind of compound can be preliminarily regarded as the inhibition against tubulin [17]. Therefore, a docking study could offer more insight into understanding the protein–inhibitor interactions and the structural features of active site of protein.

First of all, it is necessary to validate the docking reliability. We adopted the known X-ray structure of tubulin in complex with the molecular ligand **CN2** (2-mercapto-*N*-[1,2,3,10-tetramethoxy-9-oxo-5,6,7,9-tetrahydro-benzo[*A*]heptalen-7-yl] acetamide) to perform this validation. The ligand **CN2** was flexibly redocked to the binding site of tubulin and the docking conformation corresponding to the lowest energy score was selected as the most probable binding conformation. As a result, the redocked **CN2** and

Table 2
Statistical parameters of CoMFA model by PLS analysis.

Statistic index	*N*	q^2	R^2	SEE	*F*	R^2_{pred}	R^2_{bs}	SD_{bs}	Contributions %	
									Steric	Electrostatic
CoMFA	5	0.705	0.910	0.167	58.6	0.688	0.938	0.134	62.3	37.7

Note: *N* is the optimal number of components, q^2 is the leave-one-out (LOO) cross-validation coefficient, R^2 is the non-cross-validation coefficient, R^2_{pred} is the predictive correlation coefficient, SEE is the standard error of estimation, *F* is the *F*-test value, R^2_{bs} is mean R^2 of bootstrapping analysis (100 runs), SD_{bs} is mean standard deviation by bootstrapping analysis.

Table 3
CoMFA and docking results of the studied compounds.

Compound	Experimental pIC_{50}	Calculated pIC_{50}	Residual values	Docking *E* (kcal/mol)
Training set				
1	6.367	6.229	−0.138	−36.44
2	6.143	6.473	0.33	−39.88
4	6.585	6.753	0.168	−41.81
5	6.398	6.165	−0.233	−39.01
6	6.553	6.705	0.152	−34.84
7	6.745	6.555	−0.19	−36.63
9	7.125	7.133	0.008	−36.17
10	7.081	7.142	0.061	−40.93
11	6.678	6.539	−0.139	−38.14
12	7.585	7.426	−0.159	−45.17
13	7.377	7.438	0.061	−46.51
14	7.337	7.278	−0.059	−46.97
15	7.187	7.216	0.029	−38.31
16	7.119	7.287	0.168	−40.44
17	7.252	7.103	−0.149	−37.17
18	7.108	7.12	0.012	−39.34
19	6.824	6.926	0.102	−40.05
20	6.585	6.436	−0.149	−35.89
21	7.456	7.317	−0.139	−34.96
22	7.229	7.311	0.082	−31.70
23	6.268	6.636	0.368	−30.19
24	7.569	7.311	−0.258	−31.70
25	7.585	7.724	0.139	−29.63
27	7.699	7.766	0.067	−37.59
28	8.174	8.012	−0.162	−40.56
29	7.143	7.317	0.174	−36.54
30	6.553	6.445	−0.108	−33.05
31	8.260	8.051	−0.209	−38.59
33	6.658	6.718	0.06	−36.91
35	7.319	7.248	−0.071	−27.86
37	7.569	7.596	0.027	−41.48
39	7.481	7.495	0.014	−40.50
40	7.377	7.531	0.154	−38.51
41	7.367	7.353	−0.014	−42.67
42	6.62	6.602	−0.018	−31.38
Test set				
3	6.229	6.265	0.036	−42.83
8	6.553	6.862	0.309	−37.02
26	7.066	7.501	0.435	−29.31
32	8.131	7.868	−0.263	−40.36
34	7.509	7.059	−0.45	−31.74
36	7.469	7.772	0.303	−39.15
38	6.523	7.128	0.605	−37.27
43	6.377	6.449	0.072	−31.09

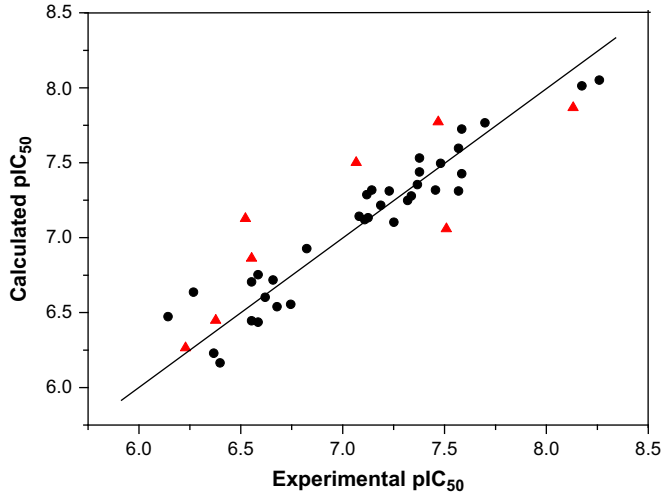

Fig. 3. Plot of calculated (predicted) activities versus experimental ones for CoMFA analysis, in which 35 compounds in the training set are expressed as dots and 8 compounds in the test set are expressed as triangles.

crystal **CN2** are almost at the same position in the active site of tubulin (see Fig. 4), suggesting a high docking reliability of DOCK 6.0. Therefore, the DOCK 6.0 docking protocol and the used parameters could be extended to search the binding conformations to tubulin for other inhibitors.

3.3. Docking results

All studied inhibitors were docked into the binding site of tubulin and the energy scores of the inhibitors are also shown in Table 3, where no precise correlations could be found between docking scores and pIC_{50} values. This observation is not surprising, because experimental pIC_{50} values are very complicated, not only relating to the target inhibition, but also dealing with a number of events. Therefore, we selected the most potent inhibitor **31** in the experiment to perform the deeper docking study and discussion below.

Here, a complete overview of receptor–inhibitor binding interactions is presented as shown in Fig. 5(a) and (b). It vividly represents the interaction model of the most potent inhibitor **31** with tubulin, in which inhibitor **31** is suitably situated at the colchicine-binding site and there are various interactions between it and the binding region of the enzyme.

The substituent R_1 is blocked by the side chains of Thr314. The *n*-pentyl of substituent R_2 is surrounded by the side chains of Pro261, Thr314, Ile347, Asn350, Val257, Asn258, Asn349 and Asn350. 1*H*-indole of the molecular frame may form a π-cation interaction with side chain NH_3^+ of Lys352, and form p–π interactions with N and O atoms of side chain of Asn258. In addition, the phenyl of the molecular frame is positioned in a large hydrophobic pocket created by side chains of Leu248, Ala250, Leu255, Ala316, Val318, Ala354 and Ile378.

3.4. Main factors affecting the activity based on a combined CoMFA and docking study

The results of CoMFA can be displayed as vivid 3D contour maps, providing an opportunity to explain the observed variance in the anticancer activity (expressed by pIC_{50}). The steric interactions are represented by green and yellow contours, and the electrostatic interactions are represented by blue and red contours.

The steric contour map of CoMFA is displayed in Fig. 6. Two big and two small yellow contours are close to the first two C atoms of

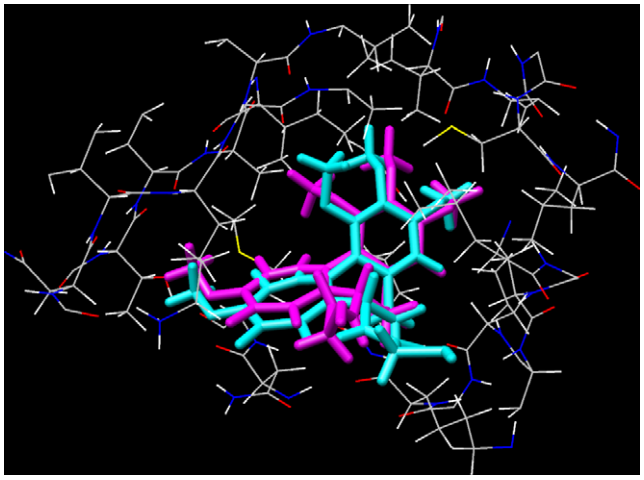

Fig. 4. Binding conformations of the redocked **CN2** (cyan) and crystal **CN2** (magenta) at the active site of tubulin. (For interpretation of the references to color in this figure legend, the reader is referred to the web version of this article.)

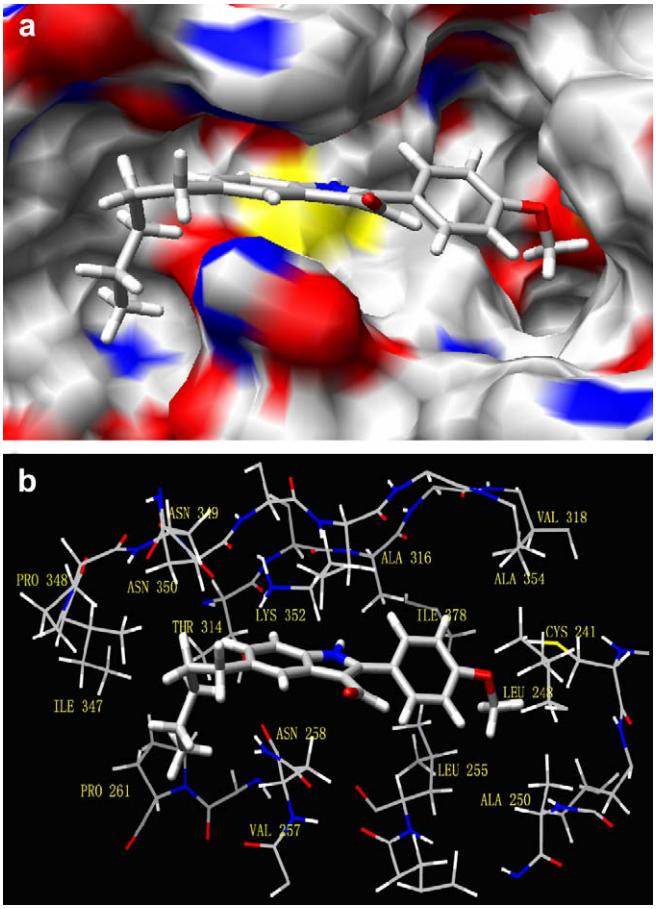

Fig. 5. (a) Docking conformation of the most potent inhibitor **31** and corresponding surface of tubulin at the colchicine-binding site, in which the red and blue regions represent oxygen and nitrogen atoms respectively, whereas white regions represent carbon or hydrogen atoms. (b) The interactions between the colchicine-binding site and compound **31**. (For interpretation of the references to color in this figure legend, the reader is referred to the web version of this article.)

substituent R_2, which are blocked by the side chains of Asn258 and Asn349. It indicates introducing ramificate alkyl as substituent R_2 can decrease the activity. Therefore, it is not strange that the activity of compound **11** is lower than that of **10**, and the activity gradually decreases from compound **28** to **30**. A large green contour is found around the terminal two C atoms of *n*-pentyl of substituent R_2, which is surrounded by Pro261, Thr314 and Ile347 that form a hydrophobic pocket. Comparing compounds **1**–**19**, **20**–**43**, we can find that the activity is strongly influenced by the length of alkyl of substituent R_2 and it increases with the length up to 4 or 5 carbon atoms. That is a possible reason why compounds **28** and **31** have higher activities than other compounds. However, there is a small yellow contour near the terminal C atom of *n*-pentyl of substituent R_2, where the residues Pro261, Thr314 are located, just as a wall blocking the prolongation of substituent R_2 of alkyl. It may be the reason why the activities of compounds **14**, **19**, **32**, **41** with substituent R_2 of *n*-hexyl are all lower than those of corresponding compounds with substituent R_2 of *n*-Bu or *n*-pentyl. In addition, there is a big yellow contour near substituent R_3 of $-OCH_3$, which is blocked by Cys241. The larger substituent R_3 (*n*-Bu) of compound **38** just falls into this yellow area, and thus this compound has quite low activity.

The electrostatic contour map of CoMFA (Fig. 7) shows two red contours. The smaller one is near the substituent R_1, and the larger one is near the first atom of substituent X. It indicates that compounds with high electronegative (i.e. low electropositive) groups on these positions would exhibit good activity. For example, compounds **4**, **9**, **25**, **33**, and **42**, which contain higher electronegative group $-OCH_3$ or halogen as substituent R_1, have higher activity than compounds **2**, **8**, **26**, **20** and **43**, which contain lower electronegative H atom. For another example, compounds **3**, **6**, **9**, **12**, **13**, **14**, and **17**–**19** with relatively lower electronegative C atom as the first atom of substituent X also show lower activity than compounds **20**, **22**, **25**, **28**, **31**, **32**, and **39**–**41** with relatively higher electronegative O atom. One bigger blue contour is found around the substituent R_2, indicating that negatively charged substituent in the area is unfavorable. The docking study also shows that the nearest residues are Asn258 and Asn349. Compounds **20** and **23** which contain electron-rich group $-OCH_3$ or –F in the substituent R_2 cannot effectively interact with electron-rich N or O atoms of Asn258 and Asn349, so they show lower activity than compounds **26**, **27**, **28**, **31** and **32** with substituent R_2 of linear alkyl. In addition, there is another large blue contour lies around the 3rd bond of R_3, suggesting that the part of R_3 falling into this area should be positively charged in favor of the activity. It is in line the result of docking analysis, because the atoms of the 3rd bond of R_3 are enclosed by some O atoms of residues,

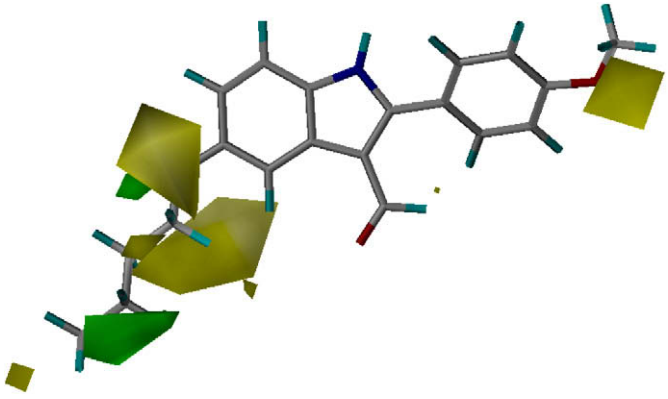

Fig. 6. CoMFA steric contour map of the most active compound **31** (green contour indicates where bulky group favors activity, whereas yellow contour indicates where small group favors activity). (For interpretation of the references to color in this figure legend, the reader is referred to the web version of this article.)

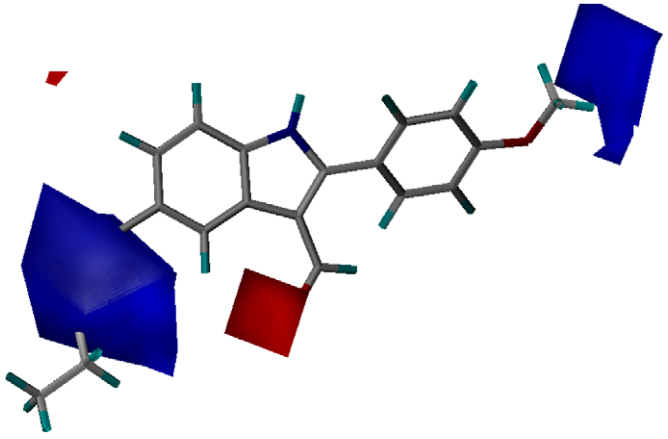

Fig. 7. CoMFA electrostatic contour map of the most active compound **31** (blue contour indicates where positive charge favors activity, whereas red contour indicates where negative charge favors activity). (For interpretation of the references to color in this figure legend, the reader is referred to the web version of this article.)

shown in Fig. 5(a). We can clearly see that the substituent R_3 of $-OCH_3$ possesses such a characteristic that its three H atoms with positive charges just falling into the blue area, whereas the substituent R_3 of $-CF_3$ possesses such a characteristic that its three F atoms with negative charges almost falling into this area. It is the reason why the activity of the compounds with R_3 of $-OCH_3$ is higher than that of the compounds with R_3 of $-CF_3$. This theoretical result can be used to explain the experimental fact that the activities of compounds **28** (8.174), **31** (8.260) and **32** (8.131) with R_3 of $-OCH_3$ are quite higher than compounds **39** (7.481), **40** (7.377), and **41** (7.367) with R_3 of $-CF_3$, respectively.

4. Conclusions

The comparative molecular field analysis (CoMFA) and docking method were synthetically applied to study a series of 2-phenylindole derivatives with anticancer activities as inhibitors towards tubulin at colchicine-binding site. The established CoMFA model shows good correlative and predictive ability in terms of high R^2 (0.910) and q^2 (0.705) as well as small SEE (0.167). Moreover, the satisfying R^2_{pred} (0.688) for an external test set composed of the eight compounds confirms the excellent predictive ability of the established 3D-QSAR model. The consistency between the CoMFA field distributions and the 3D topology structure of active site of tubulin further shows the robustness of the CoMFA model. The results from a combined 3D-QSAR and docking study are as follows. (1) Higher degree of electronegativity on the substituent R_1 (e.g., OMe, F, Cl instead of H) is favorable to the activity of the compound, because there is small red area in 3D electrostatic contour map towards it and the negatively charged R_1 should more easily perform electrostatic interaction with Thr314 in docking. (2) The substituent R_2 of linear alkyl with 4 or 5 carbon atoms in length can enhance the activity of the compound, since such a substituent can enter the green area in 3D steric contour map and it can effectively perform the hydrophobic interactions with Pro261, Thr314, Ile347 and the electrostatic interactions with Asn258 and Asn349 in docking. (3) The substituent R_3 should be selected to OCH_3-kind group which has three bond in length and whose three terminal atoms are H atoms with positive charges whereas should not be selected to CF_3-kind group whose three terminal atoms are F atoms with negative charges, because the former substituent can assort with 3D electrostatic contour map and suit with the cavum characteristic of the active site in docking whereas the latter substituent cannot. This work further shows that a combined CoMFA and docking study can provide more useful insight into understanding the QSAR of these compounds and the interaction mechanism between ligand and biotarget.

Acknowledgments

We are pleased to thank the financial support of the National Natural Science Foundation of China. We heartily thank the Molecular Discovery Ltd. for giving us the Dock 6.0 program as a freeware and the College of Life Sciences, Sun Yat-Sen University for the SYBYL 6.9 computation environment support.

References

[1] G. Bacher, T. Emig, P. Emig, T. Klenner, B. Kutscher, B. Nickel, Pure Appl. Chem. 73 (2001) 1459–1464.
[2] B. Bhattacharyya, D. Panda, S. Gupta, M. Banerjee, Med. Res. Rev. 28 (2008) 155–183.
[3] E. Pasquier, N. André, D. Braguer, Curr. Cancer Drug Targets 7 (2007) 566–581.
[4] K. Odlo, J. Hentzen, J.F. dit Chabert, S. Ducki, O.A.B.S.M. Gani, I. Sylte, M. Skrede, V.A. Flørenes, T.V. Hansen, Bioorg. Med. Chem. 16 (2008) 4829–4838.
[5] A. Jordan, J.A. Hadfield, N.J. Lawrence, A.T. McGown, Med. Res. Rev. 18 (1998) 259–296.
[6] W. Kemnitzer, J. Drewe, S. Jiang, H. Zhang, J. Zhao, C. Crogan-Grundy, L. Xu, S. Lamothe, H. Gourdear, R. Denis, B. Tseng, S. Kasibhatla, S.X. Cai, J. Med. Chem. 50 (2007) 2858–2864.
[7] A. Scuteri, G. Nicolini, M. Miloso, M. Bossi, G. Cavaletti, A.J. Windebank, G. Tredici, Anticancer Rev. 26 (2006) 1065–1070.
[8] R.J. Motzer, J. Sheinfeld, M. Mazumdar, M. Bains, T. Mariani, J. Bacik, D. Bajorin, G.J. Bosl, J. Clin. Oncol. 18 (2000) 2413–2418.
[9] W. Kemnitzer, J. Drewe, S. Jiang, H. Zhang, C. Crogan-Grundy, D. Labreque, M. Bubenick, G. Attardo, R. Denis, S. Lamothe, H. Gourdeau, B. Tseng, S. Kasibhatla, S.X. Cai, J. Med. Chem. 51 (2008) 417–423.
[10] A.M. Gaya, G.J.S. Rustin, Clin. Oncol. 17 (2005) 277–290.
[11] G.M. Tozer, V.E. Prise, J. Wilson, R.J. Locke, B. Vojnovic, M.R. Stratford, M.F. Dennis, D.J. Chaplin, Cancer Res. 59 (1999) 1626–1634.
[12] G.M. Tozer, C. Kanthou, C.S. Parkins, S.A. Hill, Int. J. Exp. Pathol. 83 (2002) 21–38.
[13] R. Gastpar, M. Goldbrunner, D. Marko, E. von Angerer, J. Med. Chem. 41 (1998) 4965–4972.
[14] M. Pojarová, D. Kaufmann, R. Gastpar, T. Nishino, P. Reszka, P.J. Bednarski, E. von Angerer, Bioorg. Med. Chem. 15 (2007) 7368–7379.
[15] D. Kaufmann, M. Pojarová, S. Vogel, R. Liebl, R. Gastpar, D. Gross, T. Nishino, T. Pfaller, E. von Angerer, Bioorg. Med. Chem. 15 (2007) 5122–5136.
[16] S.Y. Liao, J.C. Chen, L. Qian, Y. Sheng, K.C. Zheng, QSAR Comb. Sci. 27 (2008) 280–288.
[17] S.Y. Liao, J.C. Chen, L. Qian, Y. Sheng, K.C. Zheng, Eur. J. Med. Chem. (2007) 2159–2170.
[18] Y.J. Zhou, L.P. Zhu, Y. Tang, D.Y. Ye, Eur. J. Med. Chem. 42 (2007) 977–984.
[19] S.Y. Liao, L. Qian, J.C. Chen, Y. Sheng, K.C. Zheng, J. Theor. Comput. Chem. 7 (2008) 287–301.
[20] G.K. Ravindra, G. Achaiah, G.N. Sastry, Eur. J. Med. Chem. 43 (2008) 830–838.
[21] P. Yi, M. Qiu, Eur. J. Med. Chem. 43 (2008) 604–613.
[22] SYBYL 6.9 [CP], St Louis Tripos Associates, Inc., 2001.
[23] M.J. Frisch, G.W. Trucks, H.B. Schlegel, G.E. Scuseria, M.A. Robb, J.R. Cheeseman, J.A. Montgomery Jr., T. Vreven, K.N. Kudin, J.C. Burant, J.M. Millam, S.S. Iyengar, J. Tomasi, V. Barone, B. Mennucci, M. Cossi, G. Scalmani, N. Rega, G.A. Petersson, H. Nakatsuji, M. Hada, M. Ehara, K. Toyota, R. Fukuda, J. Hasegawa, M. Ishida, T. Nakajima, Y. Honda, O. Kitao, H. Nakai, M. Klene, X. Li, J.E. Knox, H.P. Hratchian, J.B. Cross, V. Bakken, C. Adamo, J. Jaramillo, R. Gomperts, R.E. Stratmann, O. Yazyev, A.J. Austin, R. Cammi, C. Pomelli, J.W. Ochterski, P.Y. Ayala, K. Morokuma, G.A. Voth, P. Salvador, J.J. Dannenberg, V.G. Zakrzewski, S. Dapprich, A.D. Daniels, M.C. Strain, O. Farkas, D.K. Malick, A.D. Rabuck, K. Raghavachari, J.B. Foresman, J.V. Ortiz, Q. Cui, A.G. Baboul, S. Clifford, J. Cioslowski, B.B. Stefanov, G. Liu, A. Liashenko, P. Piskorz, I. Komaromi, R.L. Martin, D.J. Fox, T. Keith, M.A. Al-Laham, C.Y. Peng, A. Nanayakkara, M. Challacombe, P.M.W. Gill, B. Johnson, W. Chen, M.W. Wong, C. Gonzalez, J.A. Pople, Gaussian 03, Revision D.01, Gaussian, Inc., Wallingford CT, 2005.
[24] S.J. Cho, A. Tropsha, J. Med. Chem. 38 (1995) 1060–1066.
[25] R.D. Cramer III, D.E. Patterson, J.D. Bunce, J. Am. Chem. Soc. 110 (1988) 5959–5967.
[26] I.V. Tetko, V.Y. Tanchuk, A.E. Villa, J. Chem. Inf. Comput. Sci. 41 (2001) 1407–1421.